Temperature-drift-immune wavelength meter based on an integrated micro-ring resonator

Caterina Taballione[*1], Temitope Agbana[2], Gleb Vdovin[2], Marcel Hoekman[3], Lennart Wevers[3], Jeroen Kalkman[2], Michel Verhaegen[2], Peter J.M. van der Slot[1] and Klaus-Jochen Boller[1]
[1] Laser Physics and Nonlinear Optics Group, Dept. Applied Physics, MESA+ Institute for Nanotechnology, University of Twente, 5 Drienerlolaan, Enschede 7500 AE, The Netherlands
[2]University of Delft, PO Box 5, Delft 2600 AA, The Netherlands, [3]LioniX International BV, PO Box 456, Enschede 7500 AL, The Netherlands

ABSTRACT

We present an integrated optical wavelength meter based on a Si_3N_4/SiO_2 micro ring resonator (operating over a free spectral range of ≈ 2.6 nm) whose output response is immune to temperature changes. The wavelength meter readout is performed by a neural network and a non-linear optimization algorithm. This novel approach ensures a high wavelength estimation precision (≈ 50 pm). We observe a long-term reproducibility of the wavelength meter response over a time interval of one week. We investigate the influence of the ambient temperature on the estimated wavelength. We observe an immunity of the displayed output wavelength to temperature changes of up to several degrees. The temperature-drift immunity appears to be caused by deviations from the theoretically expected (perfect) transmission function of a ring resonator, i.e., caused by deviations that are usually undesired in spectroscopic devices.

Keywords: micro ring resonators, silicon nitride, integrated wavelength meter, temperature immunity, high-precision wavelength estimation method, neural network

1. INTRODUCTION

Optical sensing devices are very important for many applications such as for finger print spectroscopy[1], in telecommunication systems[2] and as wavelength meters[3]. A spectral high-resolution is a desirable property of optical sensing devices for, e.g., spectroscopic applications[1,3]. The state of the art of high-resolution optical sensing devices includes rather big and expensive devices with critical optical stability. A waveguide integration of high-resolution optical sensing devices would offers several advantages, e.g., reduced size and long-term stability. Within the field of integrated optical sensing, devices such as micro ring resonators (MRRs) have been increasingly investigated[4-6]. The reason is that a high spectral resolution can be achieved by high-Q-factor MRRs limited only by the propagation losses. For instance, MRRs have been fabricated in Si_3N_4 technology achieving Q-values in the order of 80 million[7]. A second feature of MRRs in TripleX technology is that the resonant frequency can be tuned over one whole Free Spectral Range (FSR), for instance by thermal tuning[8]. A tunable high Q-factor MRR could be thereby used as a building block of a high-resolution wavelength meter[9], however, reproducibility of the output response is of central importance, particularly in the presence of external perturbations, e.g., temperature changes causing thermal drift.

*c.taballione@utwente.nl; phone +31 53 489 5278; lpno.tnw.utwente.nl

Integrated Optics: Physics and Simulations III, edited by Pavel Cheben, Jiří Čtyroký, Iñigo Molina-Fernández, Proc. of SPIE Vol. 10242, 1024206 · © 2017 SPIE
CCC code: 0277-786X/17/$18 · doi: 10.1117/12.2265604

A thermal drift in fact might affect the output response of the wavelength meter changing its spectral response by shifting its resonant frequencies. To improve reproducibility, various different methods are usually applied, e.g., thermal stabilization or repeated calibration with an additional reference light source of well-known and stable wavelength.
Here we present an integrated optical wavelength meter that is immune against thermal drift, within a certain temperature range, requiring no thermal stabilization or repeated calibration with additional light sources. Our approach is based on an optically integrated Si_3N_4 waveguide micro-ring resonator (MRR) the transmission of which is read out with a neural network and an optimization algorithm (smart readout). This approach is able to detect temperature changes and reduce the effect of these on the displayed output wavelength. We implement the smart readout method in an experimental setup comprising a tunable laser coupled into a MRR and a detector that measures the transmitted power. Based on transmission measurements the readout determines the wavelength of the input light. We demonstrate for the first time the full operation of such wavelength meter in that we observe long-term reproducibility (one week) and immunity to temperature changes (up to several degrees) of the displayed output wavelength. Currently the wavelength meter is operational across one free spectral range (FSR) of the MRR ($\approx$ 2.6 nm) with a high spectral resolution of $\approx$ 50 pm. An extension of the FSR appears straightforward, for instance, via exploiting waveguide birefringence of the MRR or using sequential resonators in a Vernier configuration.

2. PRINCIPLE OF DATA READOUT ALGORITHM

In order to explain the basic principle of our data readout algorithm let us consider, as an example, the measurement of an unknown wavelength of light injected into an arbitrary wavelength meter. The precision and reproducibility of the displayed wavelength are the centrally important features of a wavelength meter, but these properties can generally not be judged or verified with only a single measurement. For instance, if the output response of the wavelength meter assumes an unexpected value this can have two different reasons that are principally indistinguishable: either the wavelength meter went out of calibration or the wavelength of the injected light has changed.
This problem can be solved with a large number of measurements. With many measurements it is possible to determine and improve the calibration of the wavelength meter, and then use further measurements for obtaining knowledge also about changes of the injected wavelength. This can be illustrated with the following example where a large number of n measurements is performed with the same input wavelength, in order to obtain a distribution of values for the output response, i.e. for the displayed wavelength.
To obtain such distribution, the n measurements can be performed in parallel by dividing the available input light into n separate beams that are injected into n different wavelength meters. Alternatively, one can also perform a serial measurement by sending the light sequentially into the n different devices. The latter approach is what we have chosen for our experiments. However, we note that both approaches are equivalent because with the same total number of available input photons they yield the same signal-to-noise ratio. In any case one obtains a distribution of the displayed wavelengths that can be evaluated for characterizing the calibration and precision of the measurement.

Three types of information can be recovered from such distribution. The first is the most likely value for a common drift of all wavelength meters, which is obtained from the mean value of the distribution. The second is the overall precision obtained by the ensemble of devices, which is given by the root-mean-square (rms) deviation from the mean value. Calculating the average and rms-deviation is a straightforward technique for simple statistical data analysis. The precision is expected to improve with the number of devices, n, provided that the common drift is small, because all changes of the spectral response of the wavelength meters are uncorrelated.

Interestingly, important additional information can be obtained, namely from the observation of so-called outliers. These designate a smaller number of devices displaying a noticeably deviating wavelength as compared to the distribution of the majority of devices. These outliers indicate that the according devices have undergone a change of calibration. This information is actually very valuable because it can be used to recalibrate these devices with the mean value provided by the other measurements, which improves the overall precision of the entire set of devices for the next measurements.

We note that properly identifying outliers for recalibrating the according devices is not straightforward. Such analysis yielding an improved spectral measurement requires a sophisticated readout algorithm. The algorithm has to be capable to properly judge with what statistical weight each individual measurement has to be interpreted as an outlier, and then decide whether and how much to recalibrate (i.e. re-interpret) the response of the corresponding device. This task requires quantifying the importance of each individual measurement with regard to all the other ones.
A second issue can be that, ultimately, during the course of longer measurement series, all of the devices may be identified as outliers and become re-calibrated such that all devices will lose their original calibration. This might lead to a totally wrong wavelength display of all devices, specifically, if the drift of the devices is correlated by a common external perturbation. An example would be deliberately exposing most of the devices to a change of the ambient temperature, in order to induce a common thermal drift of their response. In this case a small number of non-drifting devices, although protected, e.g., by passive thermal shielding or active stabilization, would nevertheless be re-calibrated to display a wrong wavelength as well.

The wavelength meter we present here provides a wavelength dependence of its response via an optically integrated waveguide micro-ring resonator (MRR) on a chip. Sending the transmitted power to a photodetector generates a wavelength dependent, electrical response signal. Important is that the wavelength dependence of the response can be changed, by setting the optical length of the resonator to a number of different, predetermined values. In our experiments we set the resonator length sequentially to n different values and thereby effective realize measuring a given input wavelength with n different response functions. This resembles and mimics measuring the same input wavelength with n physically different wavelength meters. To obtain an initial set of data for a calibration we record for each of the n resonator lengths the response for a large number of known wavelengths across a range that is wider than the free spectral range of the resonator.
In order to prepare the MRR as a wavelength meter we use a multidimensional function in the form of a neural network and fit the neural network to calibration data that were obtained with the n mimicked wavelength meters. The fit yields a large number of neural network weight factors as global fit parameters that approximately comprises all information contained in the measured calibration data.
Finally, for determining the value of an unknown input wavelength, λ_u, we perform n measurements of the electric response signal, S_u^n, by setting the resonator length to the same n values as used for the calibration. Then an algorithm inserts into the neural network fit function a variety of different wavelengths, searching for a wavelength, λ_e, that would generate n signals, S_e^n, with a minimum (least-square) deviation from the n measured values, S_m^n. The found wavelength, λ_e, which minimizes the least-square deviation, is displayed as the determined input wavelength, also called best wavelength estimate for the unknown input.

A first advantage of such a smart readout is that it is not limited to a monotonously increasing or decreasing output response, which is a limitation with a standard look-up table (calibration curve of a single wavelength meter). Thereby a smart readout may widen the spectral range across which unknown wavelengths can be measured. A second advantage is that the smart readout does not rely on any specific physical property of the used optical system. As long as there is a wavelength dependent and basically reproducible response, even if the response is physically not understood or too complex for physical modeling, the smart readout can be applied to any system. There is a strong practical advantage of this black-box approach, which puts the focus only on the optical input-output relation. The optical transmission spectrum of the device does not have to be carefully optimized during fabrication and may even vary strongly from device to device. This property is what enables using integrated optical devices, as we show here, where a nanometer precision in fabrication cannot always be reached and where residual reflections at interfaces, such as with input and output fibers, cannot easily be removed. This is quite different with classical wavelength meters and spectrometers where a high precision and reproducibility in fabrication has to be guaranteed.

3. EXPERIMENTS AND RESULTS

Figure 1 shows the experimental setup (left) and the design of the waveguide resonator chip (right). As the light source we use a single-frequency external cavity diode laser (Santec, TSL-210) that is tunable from 1530 nm to 1610 nm and

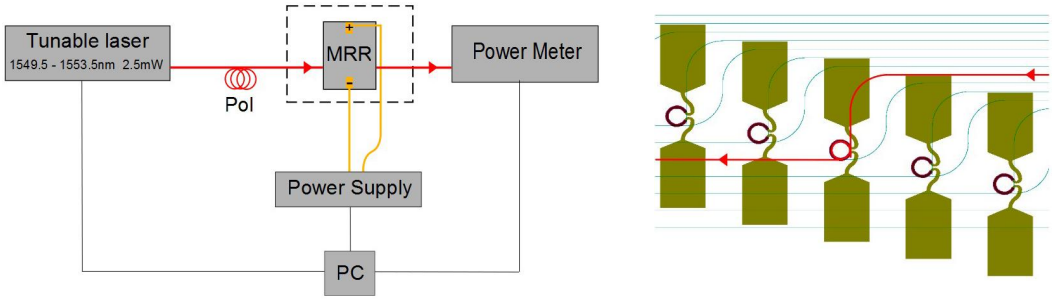

Fig. 1 (left) Experimental setup. The tunable laser, power meter and the power supply are controlled by a PC. The light from the laser is coupled into the MRR through a lensed fiber and a twisted polarizer (Pol) to control the state of polarization. A metallic box (dashed line) equipped with a resistor is built around the chip to heat up the temperature. (right) Functional design of the chip under investigation. The third ring has been chosen as illustrated. The electrodes and electric microwires (shown in gold) enable to send an electric current through heaters near designated parts of the waveguide circuit, for tuning the optical path length via thermally induced changes of the refractive index.

delivers an output of 2.5 mW from a single-mode fiber. The generated laser wavelength is available as digital output from the laser module, with an accuracy of 0.1 nm, a resolution and stability of 0.01 nm, and a repeatability of 0.05 nm, according to manufacturer specification. A twisted fiber polarizer is used to set the polarization to linear (TE). The laser light is coupled via a lensed fiber into one of the input waveguides of the chip. The micro-ring resonator is fabricated from high-contrast Si_3N_4 waveguides with a box-shaped core cross section embedded in a SiO_2 cladding which provides tight guiding and enables short resonator lengths[10]. Due to the slightly asymmetric cross section the two orthogonal polarization modes, quasi-TE and quasi-TM, have slightly different propagation constants. The radius of the resonator is 85.47 µm, which provides a free spectral range (FSR) of about 2.6 nm (≈ 323 GHz) at around 1550 nm for the TE polarization (≈ 322 GHz for TM). The input and output power coupling coefficients are designed to be in the order of 0.26, yielding a quality factor of Q ≈ 4000 (≈ 0.4 nm FWHM spectral bandwidth). In order to thermally tune the optical length of the resonators to a set of different values, a heating current can be sent through lithographically fabricated, thin-film resistor wires. Typically, applying 10 Volts with a power supply changes the resonator length by one FSR within 1 ms. Light transmitted through the resonator exiting the output waveguide is collected via a second lensed fiber, and the power is recorded with a fiber-coupled photodiode (Thorlabs, S154C). To record data over long time intervals, the laser wavelength tuning and heater voltage settings are remotely controlled, while the generated laser wavelength (received from the laser module) and the photodiode output signals are recorded, using a computer with standard software (Matlab).

First, the wavelength meter is calibrated. Starting with zero heater voltage the input wavelength is swept from 1549.5 nm up to 1553.5 nm, in steps of 0.01 nm. For each input wavelength the transmitted output power is averaged over a time interval of 300 ms, followed by averaging over 50 measurements. This measurement series is repeated for stepwise increased heating voltage, from 0 V to 10 V in steps of 0.5 V. In total the calibration data comprise 8421 values for the output power, obtained with 401 input different wavelengths and 21 different heating voltages.

The calibration data are fitted by a two-layer neural network (NN) function with 41 neurons and a total of 943 fit parameters (MathWorks, Matlab) that minimize the rms deviation from the calibration data. Figure 2 shows a comparison of the obtained NN calibration function and the calibration data, displayed vs wavelength for the 21 heating voltages. It can be seen that for each wavelength value inserted, the NN function predicts 21 power values, which lie close to the calibration data.

To test how precisely the calibrated wavelength meter estimates the wavelength of an optical input, some arbitrary wavelength within the calibration interval is injected and the transmission is recorded at the 21 settings for the heating voltages. As described in Sect.2, a search algorithm is employed that finds the wavelength for which the NN calibration function predicts 21 transmission values with the minimum squared deviation from the 21 measured values. The wavelength of minimum deviation is displayed as the estimated wavelength, i.e., the wavelength as measured by the

device. The estimated wavelength can then be compared with the true wavelength that is known from the readout of the laser module. For a comprehensive test across the entire spectral range, we perform the test sequentially with all of the

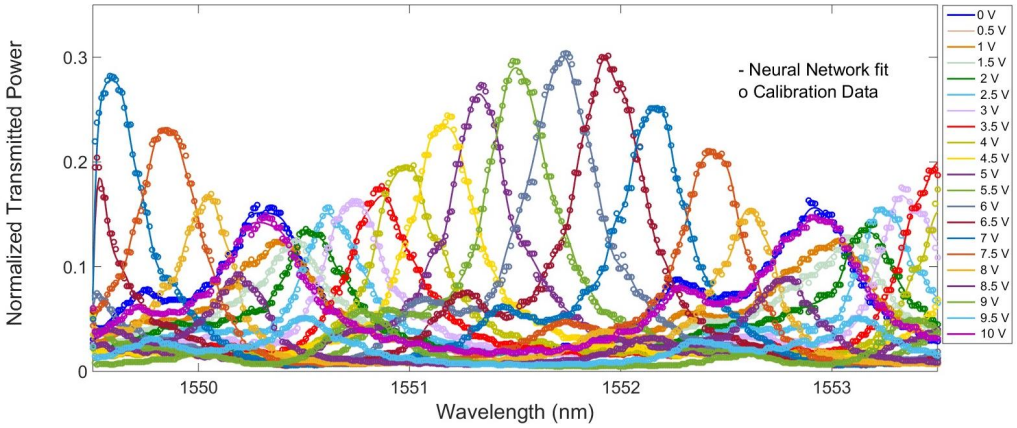

Fig. 2 The normalized calibration transmission spectra (circles) of the MRR for the 21 different applied voltages (different colors) and the fitting of the normalized calibration data by the Neural Network (solid curves). The normalization is done over the sum of the transmitted power for each wavelength.

401 input wavelengths.

We note that in our previous experiments[9] the test of the readout was carried out almost simultaneously with calibration (one millisecond delay), because the measurements aimed only on investigating the dependence of precision on the number of neurons and on the number of recorded data points. It remained thus open in how far the smart readout is reproducible also over long time intervals that are of relevance for application.

In order to investigate the longer-term reproducibility, we have performed test measurement one week after calibration.

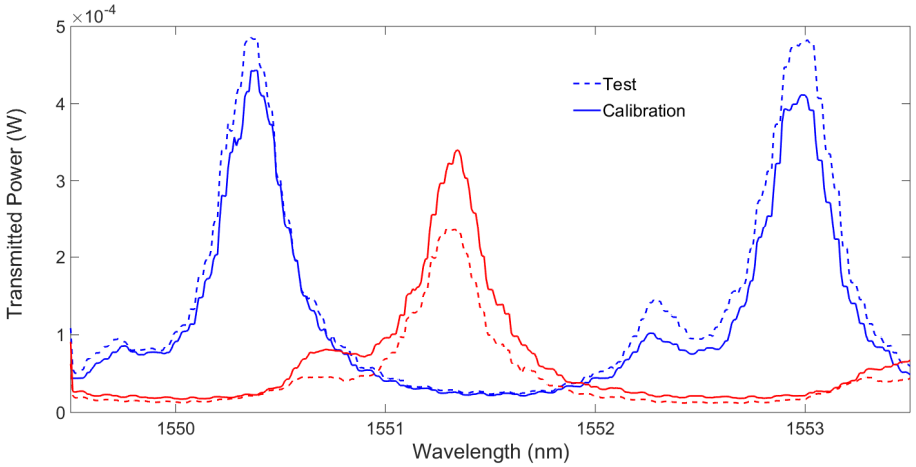

Fig. 3 Examples of transmission spectra of the MRR for two different applied voltages (blue: 0 V, red: 5 V). The thick lines represent the spectra acquired during the calibration; the dashed lines depict the data acquired during the test one week later.

A qualitative impression of the reproducibility of the recorded spectra can be obtained from Fig. 3, where for easier comparison only two examples are shown. The wavelength agreement between the spectra recorded for calibration (solid curves) and a week later (dashed curves) is very good. This can be seen from the four peak wavelengths that have remained constant within 20 pm. On the other hand there is some noticeable change in transmitted power at all main peaks which might have been caused by a drift of alignment of the free-space coupling via lensed fibers.

For a quantitative evaluation of reproducibility across the entire spectral range (1549.5 nm to 1553.5 nm) one week after calibration, the red line in Fig. 4 shows the estimated wavelength vs the known input wavelength. For comparison, the

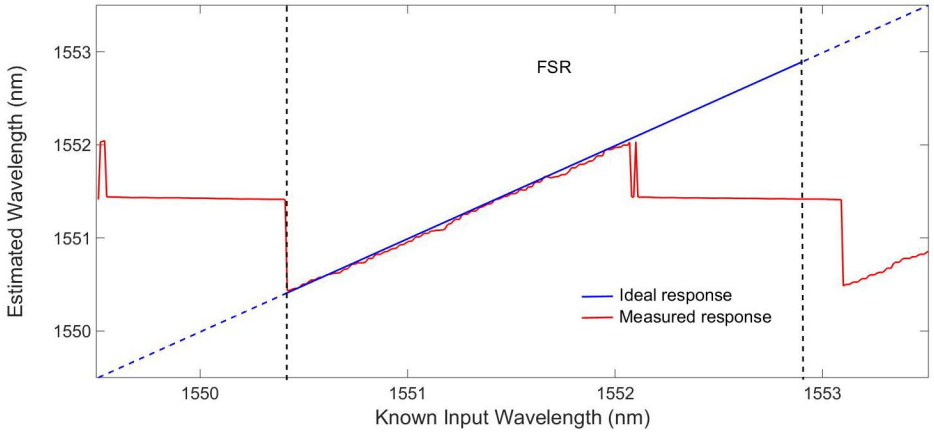

Fig. 4 Reproducibility of the output response of the wavelength meter over one-week time interval. The red curve represents the estimated wavelengths for the 401 input, supposed unknown, wavelengths. The solid blue line indicates the response of an ideal wavelength meter across the free spectral range (FSR) of the MRR where the estimated (displayed) wavelengths are exactly equal to the known input wavelengths.

blue straight line indicates the response of an ideal wavelength meter where the estimated wavelength is exactly equal to the known input wavelength. It can be seen that for central wavelengths in larger fraction of the FSR, the estimated values are very close to the ideal response, while outside the central FSR the estimation fails by giving large errors (outliers). The latter might be explained with the spectrally periodic transmission function of the MRR. The reason why

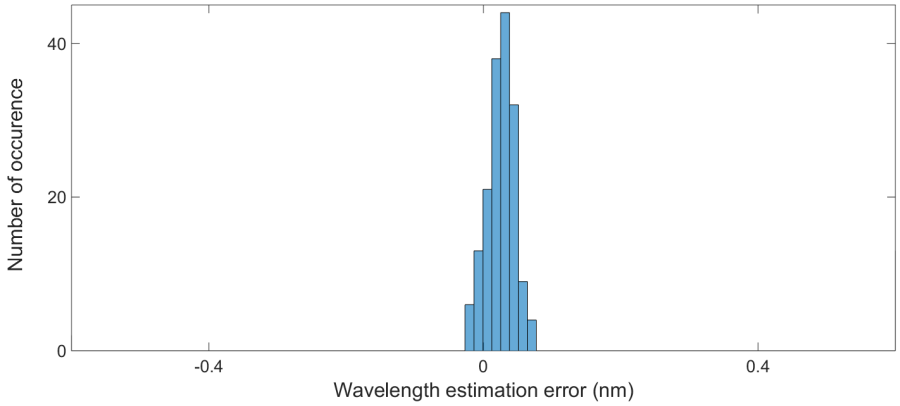

Fig. 5 Histogram of the estimation wavelength error calculated as the average difference between injected and estimated wavelengths in the central part of Fig. 4. The smart readout is capable to estimate the injected wavelengths correctly with ≈ 50 pm precision.

the estimation works correctly only in the lower two-thirds of the FSR seems to be related to how the optimization algorithm searches for the minimum standard deviation between the 21 measured values and the 21 values predicted by the NN[11].

For the wavelength range where the estimation error is small we have plotted the deviation between the injected and the estimated wavelength in a histogram in Fig 5. Determining the width of the histogram (FWHM) yields that the smart readout provides a spectral precision of about 50 pm.

As a second important investigation we measured to what extent the estimated wavelengths from the smart readout depend on external perturbations. In our experiments we selected a thermal perturbation in the form of a change in

ambient temperature. The motivation for this choice is that such thermal perturbation would provide some maximum sensitivity (worst case) scenario because the control parameter used to mimic a larger number of *n* devices is the temperature as well (temperature induced changes of the resonator length). A change in ambient temperature is expected to cause a common drift of the calibration of all the resonator transmission functions in Fig. 2. As was discussed in Sect. 2, a common drift should lead to a systematic error in the estimated wavelength that grows with the ambient temperature. To induce a controlled change in ambient temperature the wavelength meter setup was enclosed in an airflow-shielding box around the wavelength meter setup (indicated in the upper part of Fig. 1 with a dashed line), equipped with a

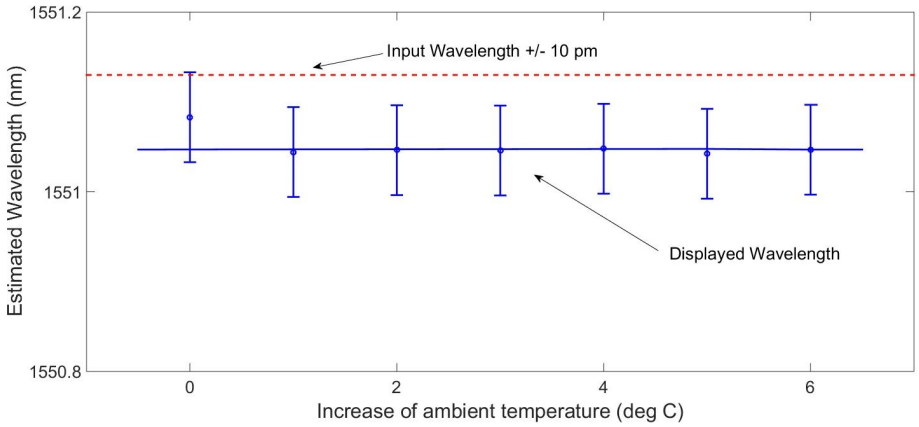

Fig. 6 Estimation of the smart readout for a single known input wavelength (red dashed line). The blue circles are the estimated values for the known input wavelength at each temperature shift. The error bar is the estimation precision obtained with the long-term interval measurements, i.e. ≈ 50 pm. The blue line is a linear fit to the data.

suspended heater and a thermocouple for air temperature monitoring. The setup allowed to increase the ambient temperature by up to 6 °C. Measurements of the transmitted powers were carried out for a single input wavelength (again 21 voltages applied to the waveguide heater) while the ambient temperature was increased in steps of 1 °C.

Figure 6 shows the wavelength meter response for a fixed input wavelength (1551.15 nm) vs the increase in ambient temperature. Surprisingly, an approximately constant response was measured as is indicated by the horizontal blue line drawn at the average displayed wavelength. The lack of a temperature dependence of the wavelength meter response means that the smart readout appears unaffected by ambient temperature changes in the investigated range. Such result is quite surprising because, as mentioned above, the spectral effect of heating the ring resonator with the chip-based heaters should be the same as heating the resonator via the external heater. The transmission curves should tune exactly the same way, which is why the smart readout algorithm should not be able to distinguish between the different experimental realizations of the same heating, because the algorithm would receive the same data at the same temperature.

4. DISCUSSION

From the previous we conclude that the smart readout is somehow able to distinguish between the temperature change induced by heating with the on-chip heaters and heating via the ambient temperature. This can only be possible if there is some additional information present in the experimental transmission spectra as compared to the theoretically expected change of transmission. It seems that an ideal ring resonator transmission spectrum (Airy transmission function) misses essential information that the experimental transmission function of a MMR on a chip is capable to offer.

In order to test this hypothesis we have calculated the temperature dependent Airy transmission of an ideal MRR with a physical model[12]. To calculate the temperature dependent effective waveguide index, we calculate the mode field distribution from the temperature dependent material indices for SiO_2 and Si_3N_4[13] and from the manufacturer specified waveguide cross section geometry. The physical waveguide length was taken from the fabrication specifications.

In Fig. 7 the calculated transmission spectra of the ideal MRR model are displayed for 21 different model temperatures. Theoretically, total temperature change of 195 °C is required to shift the spectrum by one FSR (≈ 2.6 nm). This

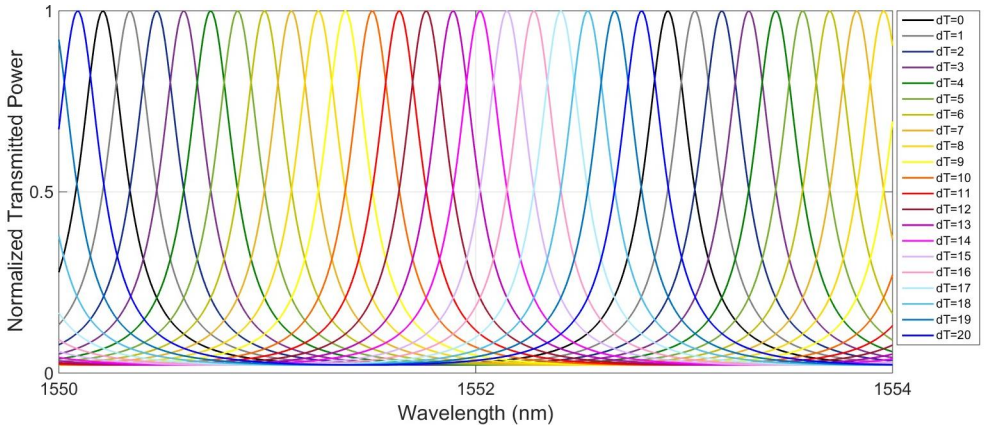

Fig. 7 Calculated transmission spectra of an ideal micro ring resonators at 21 different temperatures equally spaced over an interval of 195 °C.

corresponds to a wavelength shift of 14 pm/°C, which is in good agreement with values reported in literature[13]. The range of temperature change of 195 °C is in agreement with the experimental values typically required for tuning across one FSR. Considering that the maximum ambient temperature change was 6 °C, the wavelength shift that this change should introduce is ≈ 85 pm.

To investigate the wavelength estimation capability of the smart readout in connection an ideal resonator, we tested the NN and readout based on the ideal transmission spectra from Fig. 7. The calibration was performed with the model data at 21 model temperatures, and the wavelength readout accuracy was tested with the same range of wavelengths as in the

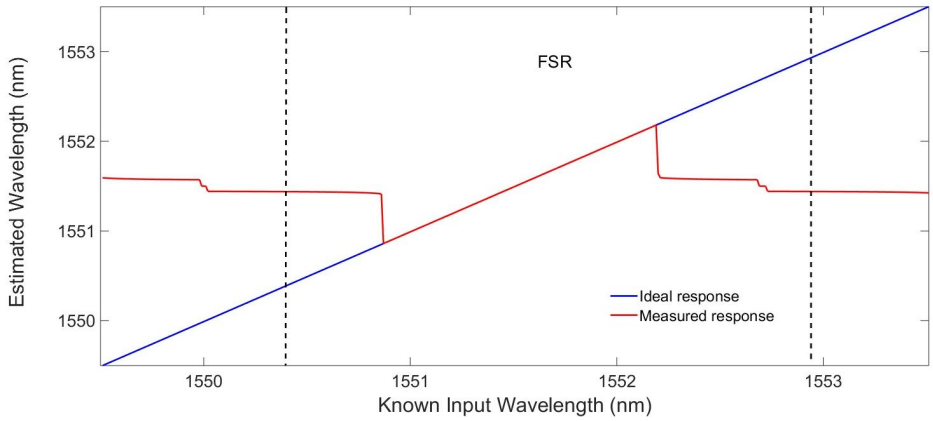

Fig. 8 Reproducibility of the smart readout for the case of a perfect ring resonator. The input and estimated wavelengths in the central spectral range agree within about 20 pm.

experiment. The comparison of the estimated wavelength vs the input wavelength is shown in Fig.8. One can see that the estimation error within the central FSR is very small (≈ 20 pm, about three-times smaller than the experimental case). These results indicate a proper performance of the smart readout also with data from an ideals model resonator.

Finally, to investigate the sensitivity vs changes of the temperature, we introduce a refractive index change corresponding to an increase of the ambient temperature of up to 6 °C, in steps of 1 °C. For each of these temperature offsets we generate the same set of spectra as in Fig. 7 that become slightly shifted from each other by 14 pm per step of

1 °C. Finally we use the smart readout to estimate the wavelength for fixed input wavelengths at the six ambient temperature configurations and from this derive the estimation error (≈ 21.5 pm).
The results are summarized in Fig. 9. For clarity we report the case of a single input wavelength (1551.74 nm). It can be seen that for an ideal MRR, with the ideal Fabry-Perot response, even small temperature changes detune the readout wavelength (although the input wavelength did not change). This result shows that the display of a smart-readout

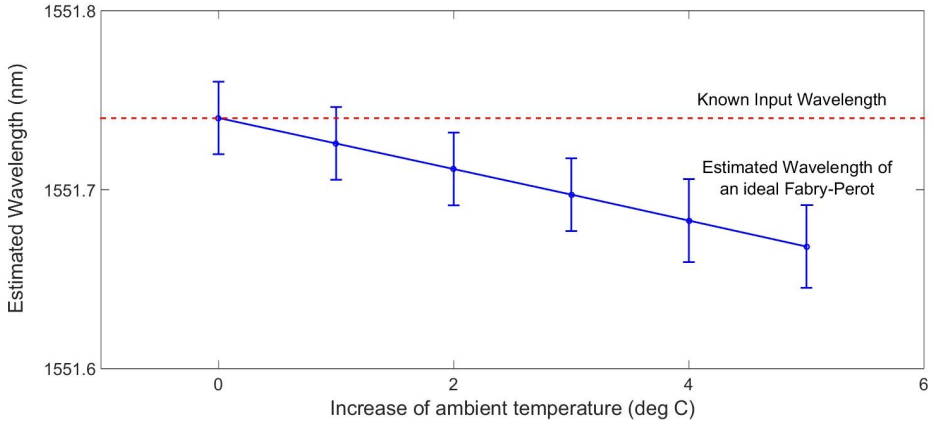

Fig. 9 Absence of temperature immunity with an ideal ring resonator. The blue circles are the estimated values for the known input wavelength (red dashed line) at each room temperature shift. The error bars are given by the estimation precision obtained at each room temperature configuration.

wavelength meter with a thermal control parameter is not immune to temperature induced perturbation, if the transmission function is ideal, such as with a model waveguide micro-ring resonator.

5. CONCLUSION

The test time interval used here (about one week) is many orders of magnitude larger as compared to previous work. This interval is long enough that the wavelength meter display might have suffered from external perturbations, for instance, thermal drift or mechanical drifts in the setup. Nevertheless we observe that the estimation precision has decreased only slightly, by about a factor of 3 (vs a 1-ms-interval), yielding a high precision of about 50 pm. This shows, for the first time, that the investigated wavelength meter approach provides a very reproducible readout also over long time intervals.
In the experiments we observed a temperature immunity of the wavelength meter, which can be quantified as follows. The ambient temperature change induced a wavelength shift of 14 pm/°C, and the experimentally induced shift is 84 pm, which is above the experimental estimation error (about 50 pm). In order to start tracking the reasons for such immunity, we showed that measurements with an ideal model does not provide immunity but display a temperature drift as expected. The cause of the experimentally observed temperature immunity is still unclear and needs to be investigated further in order to, possibly, make proper use of it.
To conclude, our approach based on a single MRR and a smart readout algorithm is open for many future developments. For instance the wavelength range to be covered could be increased with waveguide circuits of network of MRRs. Another option is increasing the resolution with ultra-low loss MRRs. Hybrid integration of passive and active waveguide platforms is also a promising field of application of our approach, such as for wavelength monitoring of hybrid lasers[14-15].

REFERENCES

[1] Rodriguez-Fernandez, C., Manzano, C. V., Romero, A. H., Martin, J., Martin-Gonzalez, M., Morais de Lima M. Jr. and Cantanero, A., "The fingerprint of Te-rich and stoichiometric Bi_2Te_3 nanowires by Raman spectroscopy," Nanotechnology 27, 075706 (2016).

[2] Early, D. A., Reth, A. D. and Rodriguez-Alvarez, O. I., "Spacecraft pointing stability constraints and instrument disturbance limits for optical remote sensing satellites," Proc. SPIE 5234, 560-571 (2004).

[3] Dey, R., Doylend J., Ackert, J., Evans, A., Jessop, P. and Knights, A., "Demonstration of a wavelength monitor comprised of racetrack-ring resonators with defect mediated photodiodes operating in the C-band," Opt. Express 21, 23450-23458 (2013).

[4] Okamoto, H., Haraguchi, M., Fukui, M. and Okamoto, T., "Optical filtering by microring resonators," Jpn. J. Appl. Phys. 42, 2692-2698 (2003).

[5] Nitkowski, A., Chen, L. and Lipson, M., "Cavity-enhanced on-chip absorption spectroscopy using microring resonators," Opt. Express 16, 11930-11936 (2008).

[6] Ramachandran, A., Wang, S., Clarke, J., Ja, S. J., Goad, D., Wald, L., Flood, E. M., Knobbe, E., Hryniewicz, J. V., Chu, S. T., Gill, D., Chen, W., King, O. and Little, B. E., "A universal biosensing platform based on optical micro-ring resonators," Biosens Bioelectron 23, 939–944 (2008).

[7] Spencer, D. T., Bauters, J. F., Heck, M. J. R., Bowers, J. E., "Integrated waveguide coupled Si_3N_4 resonators in the ultrahigh-Q regime," Optica 1, 153-157 (2014);

[8] Worhoff, K., Heideman, R. G., Leinse, A. and Hoekman, M., "TripleX: a versatile dielectric photonic platform," Adv. Opt. Techn. 4, 189-207 (2015).

[9] Oldenbeuving, R. M., Song, H., Schitter, G., Verhaegen, M., Klein, E. J., Lee, C. J., Offerhaus, H. L. and Boller, K.-J., "High precision wavelength estimation method for integrated optics," Opt. Express 21, 17042-17052 (2013).

[10] Morichetti, F., Melloni, A., Martinelli, M., Heideman, R. G., Leinse, A., Geuzebroek, D. H. and Borreman, A., "Box-shaped dielectric waveguides: a new concept in integrated optics?," J. Lightw. Technol. 25, 2579-2589 (2007).

[11] Orgun M.A. and Thornton J. (eds) [AI 2007: Advances in Artificial Intelligence. Lecture Notes in Computer Science], Springer Berlin - Heidelberg, 100-109 (2007).

[12] Kedia, J. and Gupta, N., "Mathematical modeling of ring resonator filters for photonic applications," IJARCSEE 2, 123-128 (2013).

[13] Arbabi, A. and Goddard, L. L., "Measurements of the refractive indices and thermos-optic coefficients of Si_3N_4 and SiO_x using microring resonances," Opt. Lett. 38, 3878-3881 (2013).

[14] Fan, Y., Oldenbeuving, R. M., Klein, E. J., Lee, C. J., Song, H., Khan, M. R. H., Offerhaus, H. L., van der Slot, P. J. M. and Boller, K.-J., "A hybrid semiconductor-glass waveguide laser," Proc. SPIE 9135, 91351B (2014).

[15] Fan, Y., Epping, J., Oldenbeuving, R. M., Roeloffzen, C. G. H., Hoekman, M., Dekker, R., Heideman, R. G., van der Slot, P. J. M. and Boller, K.-J., "Optically integrated InP-Si_3N_4 hybrid laser," IEEE Photon. J. 8, 1505111 (2016).